Journal Name

ARTICLE

Periodic trends and hidden dynamics of magnetic properties in three series of triazacyclononane lanthanide complexes

Received 00th January 20xx,
Accepted 00th January 20xx

DOI: 10.1039/x0xx00000x

www.rsc.org/

Elizaveta A. Suturina*[a], Kevin Mason[b], Mauro Botta[c], Fabio Carniato[c], Ilya Kuprov[d], Nicholas F. Chilton[e], Eric J.L. McInnes[e], Michele Vonci[e] and David Parker *[b]

In three structurally related series of nine-coordinate lanthanide(III) complexes (Ln = Tb, Dy, Ho, Er, Tm and Yb) based on triazacyclononane, solution NMR studies and DFT/CASSCF calculations have provided key information on the magnetic susceptibility anisotropy. Both experimental and computational approaches have revealed a poor correlation to Bleaney's theory of magnetic anisotropy. CASSCF calculations suggested that the magnetic susceptibility is very sensitive to small geometric variations within the first coordination sphere, whereas DFT analyses indicate that it is the thermal accessibility of low energy vibrational modes that may lead to distortion. Parallel NMRD and EPR studies on the three Gd(III) complexes revealed good correspondence in estimating the electronic relaxation time. The Gd (III) tris-pyridinecarboxylate complex possesses a very long electronic relaxation time making it a promising starting point for responsive gadolinium EPR probe design.

Introduction

The rich coordination chemistry of the lanthanide(III) ions continues to attract much attention, both from an experimental and theoretical viewpoint. For example, the consequences of their unique magnetic properties are being explored actively, ranging from unusual susceptibility anisotropy,[1-4] to the impact of systematic changes in the coordination environment that determine optical, NMR and EPR behaviour.[5-10] Furthermore, such work continues to encourage the development of improved computational and theoretical approaches, that may in due course allow more confident predictions to be made of spectral behaviour in solution. [11, 12]

Recently, we have been examining several series of nine-coordinate Ln(III) complexes because of their potential as cellular stains [13] and as luminescent probes, e.g. with strongly emissive Eu(III) complexes. [14, 15] Furthermore, we have been studying their behaviour as paramagnetic shift and relaxation agents, notably in responsive systems for chemical shift imaging applications.[16, 17] With this background in mind, we have undertaken a comparative study of three well-defined series of complexes, based on a triazacyclononane ring with tris-pyridinecarboxylate [18, 19] -phosphinate [20] and -amide [14] substituents (Scheme 1). These three series were chosen for this comparative study as they give rise to a small ligand field splitting, and hence provide a searching test for the analysis of the most common model of lanthanide induced paramagnetic shift, *i.e.* that proposed by Bleaney. [21,22]

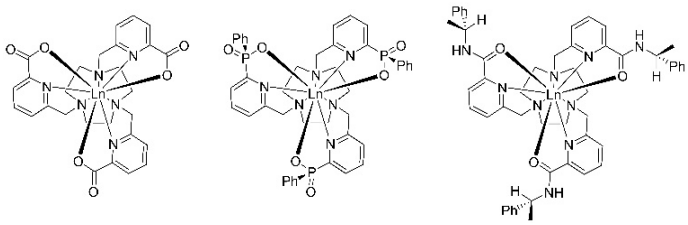

Scheme 1 Structures of [Ln.L[1]], [Ln.L[2]] and [Ln.L[3]]$^{3+}$

Bleaney's model of magnetic anisotropy assumes that the axiality (χ_{ax}) and rhombicity (χ_{rh}) of the magnetic susceptibility tensor, responsible for the pseudocontact shift (δ^{PCS}) described by eq. 1[22], can be expressed as eq.2 [21] in the high temperature limit.

$$\delta^{PCS} = \frac{1}{12\pi r^3}\left[\chi_{ax}\left(3\cos^2\theta - 1\right) + 3\chi_{rh}\sin^2\theta\cos 2\varphi\right] \quad (1)$$

$$\chi_{ax} = -\frac{\mu_0\mu_B^2 C_J B_2^0}{10(kT)^2}; \quad \chi_{rh} = -\frac{\mu_0\mu_B^2 C_J B_2^2}{30(kT)^2} \quad (2)$$

[a] Department of Chemistry, University of Bath, Claverton Down, Bath BA2 7AY, UK
[b] Department of Chemistry, Durham University, South Road, Durham DH1 3LE, UK
[c] Dipartimento di Scienze e Innovazione Tecnologica, Università del Piemonte Orientale "Amedeo Avogadro", Viale Teresa Michel 11, 15121 Alessandria, Italy.
[d] Chemistry, University of Southampton, Highfield Campus, Southampton, SO17 1BJ
[e] School of Chemistry, University of Manchester, Oxford Rd, Manchester M13 9PL

Electronic Supplementary Information (ESI) available: [NMR analyses and assignments, DFT and CASSCF studies]. See DOI: 10.1039/x0xx00000x

where C_J is Bleaney's constant, defined for each lanthanide (Tb -157.5, Dy -181, Ho -71.2, Er +58.8, Tm +95.3, and Yb +39.2), μ_B is Bohr's magneton, μ_0 is the vacuum permeability, kT is the thermal energy, B_0^2 and B_2^2 are the second order ligand field (LF) parameters. Here, the axiality is defined as 3/2 χ_z and the rhombicity is defined as $(\chi_x - \chi_y)/2$.

However, it has been shown recently that the observed proton paramagnetic shifts do not follow the trend predicted by this model for [Ln.L^1], [Ln.L^2] and [Ln.L^3]$^{3+}$, (Ln = Tb, Dy, Ho, Er, Tm, Yb).[23] For example, the ^{1}H NMR paramagnetic shifts observed in [Ln.L^1] have been found to have a very strong solvent dependence, despite the fact that no solvent is directly bound to the metal ion. Such behaviour has been attributed to very small angular perturbations that give rise to large changes in the ligand field.[24, 25]

Here, we present a systematic evaluation of experimental and theoretical work, in order to assess the impact of the ligand field variation on the magnetic and optical properties of [Ln.L^1], [Ln.L^2] and [Ln.L^3]$^{3+}$ in solution. Each of these complexes has already been reported and structurally characterised in detail. The work presented here extends our recent report of the behaviour of these systems in the solid-state. [26]

In addition, we also examine the solution behaviour of the corresponding Gd(III) complexes. Field cycling NMR (nuclear magnetic resonance) relaxometry and electron paramagnetic resonance (EPR) studies have been used to evaluate the impact of the structural permutation on the magnitude of the transverse electronic relaxation time, T_{2e}.

Results and discussion

Structures of the complexes

The complexes discussed in this paper have previously been synthesised and characterised by NMR, XRD and DFT calculations. In each of the three series of complexes, [Ln.L^1], [Ln.L^2] and [Ln.L^3]$^{3+}$, the lanthanide ion is coordinated by the three nitrogen atoms of the 1,4,7-triazacyclononane ring, three pyridine nitrogen atoms, and the three oxygen atoms of the pendant arms. The coordination sphere forms a distorted twisted tricapped trigonal prism. The complexes of [Ln.L^1] crystallise in the monoclinic Pn group, those of Ln.L^2] in monoclinic P2$_1$/n, and the series of cationic complexes [Ln.L^3](CF$_3$SO$_3$)$_3$ crystallise in the trigonal R$_3$ space group. [13,14,20,22]

.

The helicity about the lanthanide centre is opposite to the sense of the triazacyclononane ring chirality, specifying the chirality associated with the layout of the pendant arms and the local chirality of each NCCNLN chelate, *i.e.* Λ-$\delta\delta\delta$/Δ-$\lambda\lambda\lambda$ for each complex. The other stereoisomer (Δ-$\delta\delta\delta$/ Λ-$\lambda\lambda\lambda$) features an unfavourable repulsive interaction between the CH_2 group of the nine-membered heterocycle and the pyridine ring. The rate of exchange in solution between enantiomers was found to be slow on the NMR timescale at room temperature. [14,20,22] The chirality at each stereogenic phosphorus centre in [Ln.L^2] is the same, giving rise to *RRR*-Λ-$\delta\delta\delta$/*SSS*-Δ-$\lambda\lambda\lambda$ enantiomers, where the phenyl rings are directed upwards, sterically protecting the lanthanide ion. In the alternate diastereoisomer, *i.e. SSS*-Λ-$\delta\delta\delta$/*RRR*-Δ-$\lambda\lambda\lambda$ the phenyl rings are pointing down: this structure was not observed.

The L^3 ligand has a stereogenic centre at carbon, and was prepared as either the *R* or *S* enantiomer.[13,14] In the crystal structures of [Ln.L^3](CF$_3$SO$_3$)$_3$, only one diastereoisomer (*RRR*-Λ-$\delta\delta\delta$/*SSS*-Δ-$\lambda\lambda\lambda$) was observed. However, solution NMR analysis revealed the presence of a minor diastereoisomer (*SSS*-Λ-$\delta\delta\delta$/*RRR*-Δ-$\lambda\lambda\lambda$). Measurements of water proton relaxivity in aqueous solutions of the corresponding gadolinium complexes for each of these three ligands indicated that there are no solvent molecules in the first coordination sphere, a conclusion that was confirmed by measurements of the rate of decay of the lanthanide excited state in water and D_2O. [13,20,22]

The Ln-N and Ln-O bond lengths vary between the [Ln.L^1], [Ln.L^2] and [Ln.L^3]$^{3+}$ complexes. And, within the series all of the Ln-donor atom bond lengths get shorter from Tb to Yb, in keeping with the lanthanide contraction. Not all of the complexes under consideration in this paper have an X-Ray diffraction (XRD) structure, but we can compare the density functional theory (DFT) optimized structures for each of them (Tables S2-S5). The bond lengths for the optimised structures were found to be slightly longer than those found in the XRD structures. The Ln-O bond length is the longest in the L^3 series (2.36-2.42 Å) according to both DFT and XRD (2.34-2.38 Å); shorter values for the Ln-O bond were found in complexes of L^2 (2.24-2.33 Å) and L^1 (2.31-2.39 Å). The Ln-N(ring) bond is shorter than the Ln-N(pyridine) bond in complexes of L^1 (2.48-2.54 vs. 2.62-2.71 Å) and L^3 (2.48-2.56 vs. 2.56-2.66 Å) but they are almost the same in the complexes of L^2 (2.59-2.67 and 2.61-2.68) (Figure 1).

Journal Name

ARTICLE

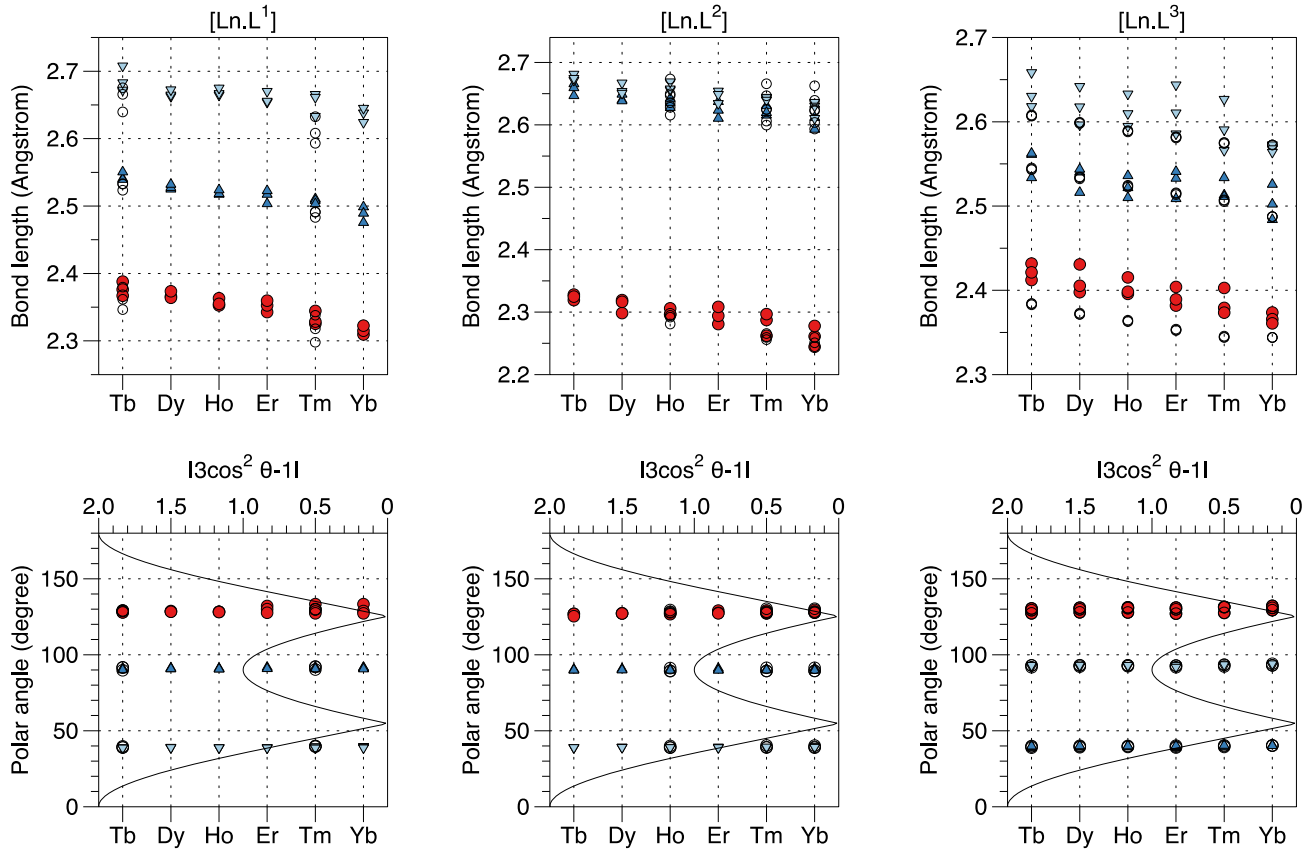

Figure 1 Structural parameters of the first coordination sphere of (*left*) [LnL^1], (*centre*) [LnL^2] and (*right*) [LnL^3]$^{3+}$: bond lengths (*top panels*) and polar angles (*bottom panels*) were computed by DFT (M06-2X/cc-pVDZ/Stuttgart-ECP, SMD methanol). The oxygen coordinates are shown in red circles, pyridine nitrogen – dark blue up-triangles and 9-N_3 ring nitrogen – light blue down-triangles. The angular dependence of the $|Y_{20}|$ spherical harmonic is shown for guidance to assess the contribution to B_0^2 from different coordination sites. Parameters from crystal structures determined at 120K are shown as empty circles for comparison. [13,14,20,22]

The polar angle of the oxygen atom is very close to the magic angle, where the second rank spherical harmonic Y_{20} crosses zero, so its contribution to the B_0^2 ligand field parameter is expected to be small, but very sensitive to any angular variation. [24] Contributions arising from the ring and pyridine N atoms to the ligand field parameter B_0^2 have the opposite sign but a similar amplitude, so they compensate each other, meaning that the small contributions from the oxygen atoms to B_0^2 can change its sign (Figure 1).

Each DFT optimised structures features distortion from C_3 symmetry, due to the very flat potential energy surface, manifested in the appearance of about twenty normal modes under 100 cm^{-1}. The other reason for this distortion may be the presence of a nearly orbitally degenerate ground state for some of the lanthanides that leads to difficulties in SCF convergence. Available crystal structures for [Ln.L^1] and [Ln.L^2] also reveal a distortion from C_3 symmetry due to packing, but in [Ln.L^3] the C_3 axis coincides with the R_3 unit cell axis, so that any random distortion is averaged out leading to apparently ideal C_3 symmetry.

Emission spectral behaviour of Eu(III) complexes

The emission spectra of [Eu.L^1], [Eu.L^2] and [Eu.L^3] were measured in methanol at room temperature (Figure 2), revealing the difference in the ligand field. The splitting of the $^5D_0 \rightarrow {}^7F_1$ band (inset, Figure 2) is well known to be proportional to B_0^2. However, resolution of the multiplet was only observed for [Eu.L^1] (B_0^2 = -100 cm^{-1} in Stevens formalism) [27] and in the case of [Eu.L^2], only limits to the splitting can be estimated, i.e., $|B_0^2|$ < 100 cm^{-1} whereas for [Eu.L^3] , $|B_0^2|$ < 130 cm^{-1}. The lifetime of the Eu(III) excited state in emission spectroscopy is ~1000 μs, meaning that the estimated ligand field is averaged over molecular vibrations.

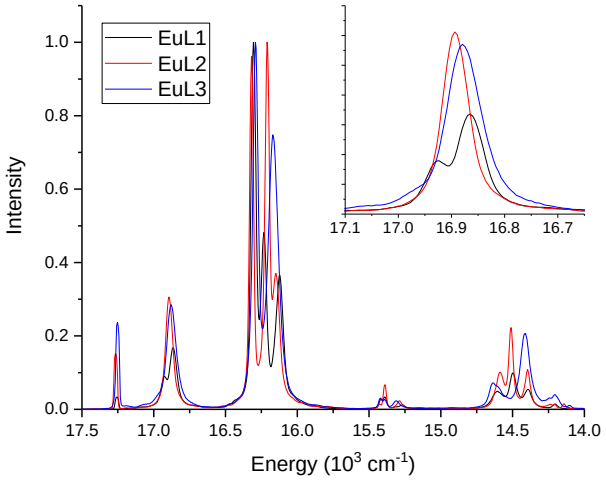

Figure 2 Room temperature emission spectra of [Eu.L[1]] [Eu.L[2]] and [Eu.L[3]]$^{3+}$ in methanol, showing the splitting of the ΔJ = 1 manifold (inset). These spectra are quite different in water, where the ligand field splitting of [Eu.L[1]] for example, is exactly half of that observed in methanol. [12]

Circular polarized luminescence (CPL) spectra for [Eu.L[1]] and [Eu.L[2]] were recorded in methanol but did not provide resolution of the $^5D_0 \rightarrow {}^7F_1$ band because the A-A and A-E transitions are of the same sign in CPL. With [Eu.L[3]], in contrast, the presence of positive and negative CPL components in this transition allowed a more accurate estimate to be made for $|B_0^2|$= 115 cm^{-1} (Figure S4).

NMR assignment and fitting

Analysis of proton NMR spectra of these complexes in solution suggested that each structure has time-averaged C_3 symmetry, with up to nine identifiable resonances in the case of complexes of L[1], twelve in the case of L[2] and fifteen in the case of L[3]. The total spectral width of the proton NMR spectra varied in a non-systematic way (Figure 3, Figure S3).

All of the spectral information for each complex, together with proton assignments are presented in Figure S3 and Table S1. Assignments and fitting procedures were performed using the averaged dipolar hyperfine tensors computed with DFT, as described by eq. 18 found in the work of Kuprov [28]. In that work, eq 18 is equivalent to eq. 1 for a point electron spin.[29] Proton dipolar hyperfine tensors computed by DFT were found to be similar to values found using the point-dipole approximation. Attempts were made to include the contact contribution to the fit, by including the isotropic parts of hyperfine and magnetic susceptibility tensors. However, this led to a marginal improvement in the fit only in the case of [Ho.L[2]] (Table S5), where the isotropic magnetic susceptibility was found to be 0.97 Å^3 – very close to the theoretical value.

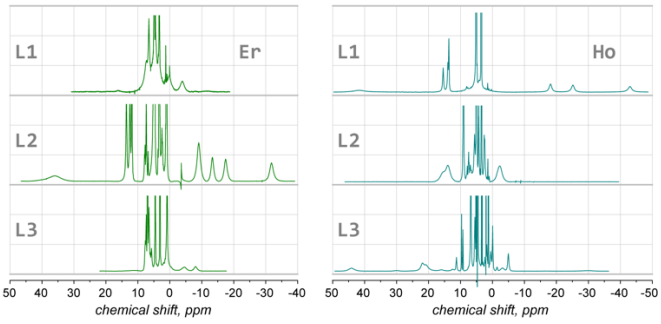

Figure 3 ^{1}H NMR (700 MHz, CD_3OD, 295K) spectra of ErL[1], ErL[2], ErL[3] and HoL[1], HoL[2], HoL[3] showing the absence of any obvious systematic variation in the total spectral width.

The axiality of the susceptibility tensor that was extracted from the NMR fitting analysis showed significant deviations from Bleaney's model, if the ligand field parameter B_0^2 is assumed to be constant within each series (Figure 4). By plotting χ_{ax}, versus the Bleaney constant C_J , rather than the chemical shift of a specific atom, the possibility of an incorrect assignment or shift variation due to a change in the relative position of that atom can be eliminated.[23]

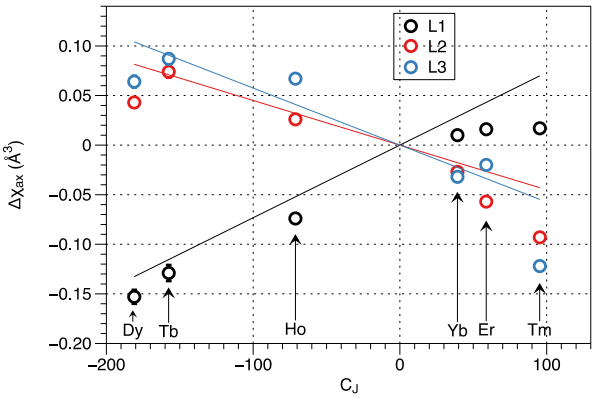

Figure 4 Axiality of the magnetic susceptibility tensor (Å^3 SI units), extracted from the room temperature ^{1}H NMR spectra, plotted against the Bleaney constant C_J for each lanthanide. A linear fit, predicted by Bleaney's model (*line*), shows a rather poor correlation with the experimental data (*circles*).

If Bleaney's model is followed, a linear fit of the data presented in Figure 4 should be obtained. Analysis of the 'best' slopes in Figure 4 show that the B_0^2 sign for L[1] complexes is negative (–340 cm^{-1}), while for complexes of L[2] and L[3], B_0^2 is positive (+240 cm^{-1} and +290 cm^{-1}, respectively). However, the fits are poor, and the main reason is likely to be the variation in the average value of B_0^2 across each lanthanide series.

Magnetic susceptibility tensor analysis

In our recent published work, we have shown that the axiality of the susceptibility tensor in C_3 symmetric structures is very sensitive to the polar angles of the Ln-O bonds because they are very close to the magic angle (Figure 1). [24-26]

In the asymmetric structures predicted by DFT, the three polar angles and the bond distances are slightly different, but in solution that variation is likely to be averaged out. However,

the small asymmetry strongly affects the susceptibility tensor and, hence the pseudocontact shift (PCS) field in a dramatic way.

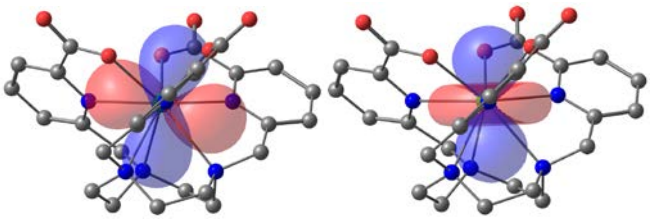

Figure 5 Comparison of the PCS field 200 ppm iso-surfaces (blue – negative shift, red - positive shift) for the DFT optimised structures of [Yb.L^1] ; (*left)* without symmetry constraint and (*right)* the symmetrised one. Images were generated with Chemcraft software.

The small asymmetry of the optimised structures (Figure 1) leads to a pronounced tilting of the main magnetic axis with respect to the approximate C_3 symmetry axis, and the development of considerable rhombicity (maximum $\chi_{rh}/\chi_{ax} = 1/3$) (Figure 5, Table 1).

Table 1 Magnetic susceptibility tensors computed with CASSCF/RASSI/SINGLE_ANISO at T=295 K for DFT optimised structures without symmetry constraints. The tilt angle corresponds to the angle between the approximate C_3 axis and the main magnetic axis.

Ln	χ_{ax}(Å^3)			χ_{rh}/χ_{ax}			tilt angle (°)		
	L1	L2	L3	L1	L2	L3	L1	L2	L3
Tb	0.05	-0.05	0.15	0.20	0.29	0.04	79	100	5
Dy	0.02	0.12	0.15	0.33	0.17	0.15	106	22	7
Ho	-0.05	-0.02	0.07	0.03	0.27	0.13	2	67	6
Er	-0.08	-0.09	-0.06	0.20	0.06	0.07	7	9	1
Tm	0.11	-0.13	-0.15	0.25	0.05	0.09	104	10	4
Yb	0.03	-0.05	-0.05	0.30	0.14	0.17	77	16	2

The distortion from C_3 symmetry cannot have a preferred direction for an isolated molecule. For example, if distortion is directed to one of the coordinated oxygen atoms (O1), two other structures with exactly the same distortion in the direction of O2 and O3 will have the same energy. The average over those structures (assuming fast exchange on the NMR timescale) leaves only the χ_0^2 component of the susceptibility tensor, projected onto the C_3 axis.

In the high temperature limit (eq. (2)), χ_{ax} is proportional to the ligand field parameter B_0^2, which in a simple point-charge crystal field model can be related to the geometric positions of the coordinating atoms $B_0^2 \sim \Sigma_i r_i^{-3}(3\cos^2\theta_i - 1)$, where r_i, θ_i are coordinates of the ligand. It is clear that χ_{ax} is non-linear with respect to the displacement of atoms in the first coordination sphere, so the average axiality value of the susceptibility tensor will be $\langle\chi_0^2\rangle \sim \langle B_0^2\rangle \sim \langle\Sigma_i r_i^{-3}(3\cos^2\theta_i - 1)\rangle \neq \Sigma_i\langle r_i\rangle^{-3}(3\cos^2\langle\theta_i\rangle - 1)$. Hence, if low-symmetry geometries occur on a timescale faster than the NMR experiment but slower than that of electron relaxation, only the average $\langle B_0^2\rangle$ value can be extracted, but we cannot quantify average theta angles, nor average metal-ligand bond distances based on the mean anisotropy of the magnetic susceptibility.

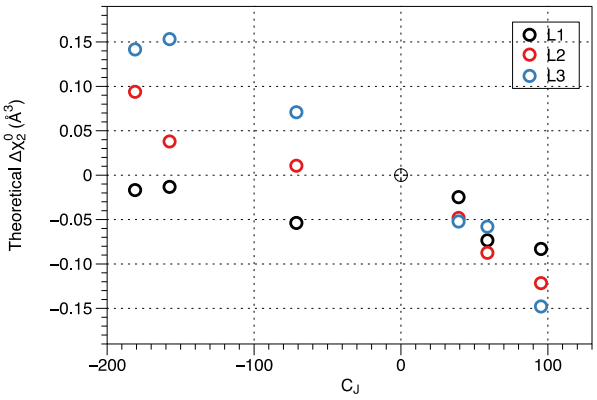

Figure 6 Averaged anisotropy of the susceptibility tensor computed with CASSCF/RASSI/SINGLE_ANISO for optimised DFT structures, showing the deviation from Bleaney's linear model due to structural variations within each ligand series.

This averaged magnetic anisotropy (Figure 6, Table 1) does not have a linear dependence on C_J. Even the calculations for symmetric structures show deviations from the linear behaviour that is predicted by Bleaney's model. However, these deviations are caused by the variation of the ligand field parameter, and if we allow for that, Bleaney model holds up relatively well, (Figure S2).

Out of the three series, the computed magnetic susceptibility anisotropy of the complexes of L^3 is better described by eq. 2 compared to those in the L^1 and L^2 series, despite the significant distortion from the C_3 structure in their optimised geometries. The reason for such behaviour may tentatively be ascribed to the longer Ln-O bond in the complexes of L^3 that suppresses the impact of the angular variation of the magnetic susceptibility anisotropy since $B_0^2 \sim r^{-3}$, resulting in a smaller tilt angle variation of the main magnetic axis (Table 1).

There is a qualitative agreement in the variation of the averaged axiality value χ_0^2 within the L^3 and L^2 series with the experimental value of χ_{ax} , (Figure 4). However, the computed values of χ_0^2 for complexes of L^1 in methanol are much smaller than those determined from the experimental data. Such a disagreement is not typical of behaviour using this theoretical approach. A much better agreement between computed and experimental data for 8-coordinate lanthanide complexes has been reported, for example.[27]

In previous work,[24] we have shown that lanthanide complexes of L^1 in water have a much smaller anisotropy than in methanol (about one half), for example, χ_{ax}= –0.053 Å^3 for Dy, –0.063 Å^3 for Tm and –0.013 Å^3 for Yb. The implicit solvation model used in the calculations reported here does not capture the structural differences of L^1 in water and methanol that would lead to such a dramatic solvent dependence. The

molecular electrostatic map (Figure S1) shows that the oxygen donor site in L^1 is clearly the most exposed for interaction with solvent molecules.

Static structural differences may not be the only issue to consider in assessing the discrepancy of these computed and experimental values. Vibrational averaging over the normal modes that change the magnetic susceptibility tensor also has to be considered, provided that these modulations are slower than the rate of electron relaxation. Electron relaxation rates for these complexes typically range between 10^{12} to 10^{13} s^{-1},[30] meaning that vibrations of up to 100 cm^{-1} need to be considered. DFT calculations suggest that there are a number of such 'soft' modes accessible in this rang that can modulate the magnetic susceptibility tensor (Table S6).

^{1}H NMR Relaxation analyses in water of [Gd.L$^{1-3}$]

The nine-coordinate Gd complexes of L^1, L^2 and L^3 in water can be viewed as classical 'outer sphere' magnetic resonance (MR) contrast agents, as they lack a coordinated water molecule. In such complexes, only the outer sphere mechanism of relaxation normally needs to be considered. It involves electron-nuclear magnetic dipole coupling that occurs when the solvent molecules approach the metal centre during their translational diffusive motion. Usually, it is described by Freed's analysis[31] and depends on the distance of closest approach, a, the translational diffusion coefficient, D, and the electronic relaxation times $T_{1,2e}$. It is customary to describe the electron spin relaxation of the Gd(III) ion as arising from a modulation of the transient zero-field splitting (ZFS) due to distortional motion. In this model, the values of $T_{1,2e}$ are expressed in terms of the mean squared fluctuation of the ZFS, Δ^2, and of the correlation time, τ_v, that is associated with the distortional motion. It is reasonable to hypothesise that a fluctuation in the metal complex coordination polyhedron may arise from solvent encounters, *e.g.* when changing the transient hydrogen bonding between the solvent and the ligand. [25,31]

Proton nuclear magnetic relaxation dispersion (NMRD) profiles were recorded at 10, 18, 25 and 37 °C in the proton Larmor frequency range from 0.01 to 70 MHz (Figure 7). Analysis of the NMRD profiles gives information on the parameters that affect the observed relaxivity (Table 2). A simultaneous fit of the four NMRD profiles of [Gd.L^1] has been performed to Freed's model of the outer-sphere contribution to relaxivity,[31] using as variable parameters Δ^2, τ_v, a and the activation energy of τ_v (E_D) and of the diffusion coefficient (E_D).

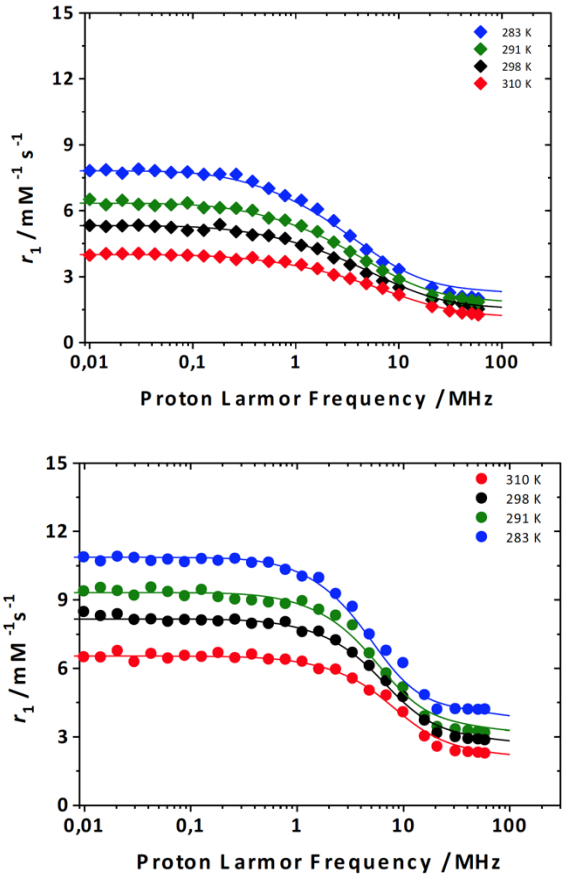

Figure 7 ^{1}H NMRD profiles of [Gd.L^1] (0.34 mM; pH 6.9) – *top*, and [Gd.L^3]Cl_3 (0.59 mM; pH 6.4) – *bottom* measured at different temperatures (283, 291, 298 and 310 K). The curves were calculated with the parameters shown in Table 2.

Table 2 Relaxation parameters obtained from the NMRD fitting analysis. Here, r_1 is the paramagnetic relaxivity, r is the average distance between Gd and the second sphere water protons, τ_R is the molecular rotational correlation time and τ_M is the second sphere water exchange lifetime.

	Outer Sphere and Second Sphere parameters (298 K)			
	[Gd.L^1]	[Gd.L^3]Cl_3	[Gd.L^2] [a,e]	[Gd.DOTA(H_2O)] [b]
r_1^{20} ($mM^{-1}s^{-1}$)	1.94	3.15	1.93	2.33
Δ^2 (s^{-2}; ×10^{19})	2.4±0.2	1.1±0.1	2.9±0.1	1.6
τ_v (ps)	1.0±0.2	14±1	10±1	11
E_V (kJ/mol)	3.3±1.2	6.1±1.8	5.0±1.2	1
q'	/	3*	/	/
r (Å)	/	3.66±0.14	/	/
τ_R (ps)	/	44±3[c]	/	/
τ_M (ns)	/	0.14±0.0[d]	/	/
a (Å)	4.38±0.11	4.30±0.09	4.20±0.08	3.7*
D ($cm^2 s^{-1}$;×10^5)*	2.24	2.24	2.24	2.24
E_D (kJ/mol;)	19.5±0.7	20.5±1.2	21.0±1.1	20.2

* fixed during the fitting; [a] results of a new simultaneous least-squares fit of the data taken from reference [32]; [b] From reference [33]; [c] the calculated value of the activation energy E_R is 14.7±0.5 (kJ/mol); [d] the calculated value of the activation energy E_M is 1.1±0.2 (kJ/mol)); [e] data for [Gd.L^2] is given for the P-Me analogue , [22] as [Gd.L^2] is not water soluble.

The value of the "outer sphere" distance a was allowed to vary only within the range 3.8-4.6 Å. On the other hand, the profiles for [Gd.L^3]$^{3+}$ have been fitted to allow for a contribution from

the *second sphere* of hydration. In this case, the relaxivity also depends on the number *q*' of second-sphere water molecules, their average distance from the paramagnetic centre (*r*), their exchange lifetime τ_M and its activation energy (E_M) and the molecular rotational correlation time τ_R and its activation energy (E_R). The number of second-sphere (SS) water molecules, *q*', has been arbitrarily fixed to three, in accordance with the C_3 symmetry observed by solution NMR. The other parameters were allowed to vary within a reasonable range of values.

The low-field relaxivity of [Gd.L^1] (0.01 to ~6 MHz) is relatively high because of the small value of Δ^2 and τ_V, consistent with a long electronic relaxation time at zero-field, τ_{S0}, eq. 3. [34, 35]

$$\frac{1}{\tau_{S0}} = \frac{\Delta^2\left(4S\left(S+1\right)-3\right)\tau_V}{5} \qquad (3)$$

Only [Gd.DOTA(H$_2$O)]$^-$ (DOTA = 1,4,7,10-tetraazacyclododecane-1,4,7,10-tetraacetic acid) and related complexes show comparable values for these parameters. In aqueous media, the [Ln.DOTA(H$_2$O)]$^-$ complexes assume either a capped square antiprismatic (SAP) or a capped twisted square antiprismatic (TSAP) geometry, where the lower square plane is occupied by the four amine nitrogen atoms, the upper plane is defined by the four carboxylate oxygen atoms, and the capping position is occupied by a water molecule. The two geometries differ for the relative orientation of the two square planes. This represents a highly symmetric and very rigid chelate structure with long-lived metal-nitrogen and metal-oxygen bonds.[36] It was concluded, from early experimental observations, that high symmetry and increasing structural rigidity are associated with long values of electronic relaxation.[37] In fact, DOTA-type chelates exhibit longer τ_{s0} (smaller Δ^2) values than all other Gd(III) compounds studied. The τ_{S0} values are 3.47, 0.54 and 0.47 ns for [Gd.L^1], [Gd.L^3]$^{3+}$ and [Gd.DOTA(H$_2$O)]$^-$, respectively; the low-field relaxivity of [Gd.L^1] and the calculated outer-sphere relaxivity of [Gd.DOTA(H$_2$O)]$^-$ are nearly identical. The shorter electron relaxation time in [Gd.DOTA(H$_2$O)]$^-$ is compensated by the shorter distance *a*. The complexes [Gd.L^1] and [Gd.L^3]$^{3+}$ have the longest electronic relaxation times τ_{s0} reported.[38]

The high field relaxivities (>10 MHz) of [Gd.L^1] and [Gd.L^2] are relatively low because of the larger value of the average distance *a*, between outer sphere water molecules and the Gd^{III} ion. For [Gd.L^3]$^{3+}$, higher values of relaxivity are reasonably attributed to a significant second sphere contribution to the observed relaxivity, in which water molecules reside for longer, on average, near to the Gd centre because of hydrogen bonding to the amide carbonyl oxygen (a H-bond acceptor) and to the amide NH groups as H-bond donors). The temperature dependence of the relaxivity allowed an estimation of the enthalpy change associated with solvent diffusion, and a value for ΔE_D of -20(±1.0) kJmol^{-1} was found for [Gd.L^1] and [Gd.L^3]$^{3+}$, based on standard Arrhenius analysis (Table 2).[31]

Solution EPR spectroscopy

EPR measurements were performed for each gadolinium complex at 9.4 GHz (0.35 T, 14.9 MHz for ^{1}H, Figure 8). The T_{2e} values can be estimated from the linewidth, according to a well-established equation, eq. 4,[39, 40]

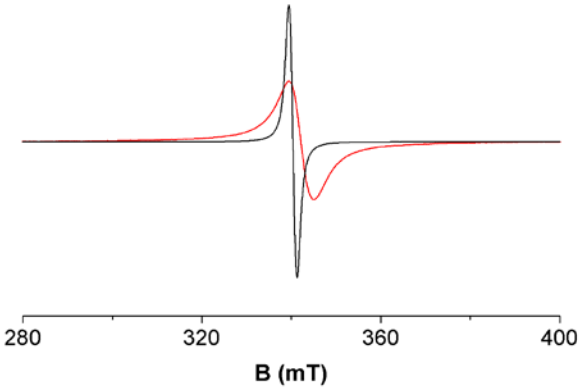

Figure 8 EPR spectra of aqueous solutions of [Gd.L^1] (*black*; 0.34 mM) and [Gd.L^3]Cl$_3$ (*red*; 0.59 mM) at 298 K and neutral pH.

$$\frac{1}{T_{2e}} = \frac{\Delta H\sqrt{3\pi}g\beta}{h} \qquad (4)$$

Table 3 EPR Parameters for [Gd.L^1] and [Gd.L^3]$^{3+}$ (291 K, 0.35 T, X-band, ~9.4 GHz)

Complex	ΔH_{pp}/mT	T_{2e}/ns	*g*
[Gd.L^1]	1.74	3.8	1.9950
[Gd.L^3]$^{3+}$	5.74	1.1	1.9932
[Gd.DOTA(H$_2$O)]$^-$ [a, 41]	8.10	0.7	1.9705
[Gd.DOTA(H$_2$O)]$^-$ [b, 42]	8.23	0.8	1.9862

[a] Data from Clarkson and Freed at 295K, (1998), who stated that the value of ΔH_{pp} = 81 G; *g* = 1.9705.[41]

[b] New measurement under identical conditions as for [Gd.L^1-L^3]. In A. Borel *et al.*[42, 43] a *g* value 1.9926 was reported for [Gd.DOTA(H$_2$O)]$^-$ (298 K)

The T_{2e} values can also be evaluated from the NMRD relaxometric parameters. Therefore, a simulation of the frequency dependence of T_{2e} was undertaken, according to Solomon-Bloembergen-Morgan (SBM) theory using the best-fit parameters from the NMRD data for [Gd.L^1] and [Gd.L^3]$^{3+}$, (Figure 9).[34] The agreement between the values obtained from the EPR and NMRD data is very good (Table 3, Figure 9), supporting their reliability.

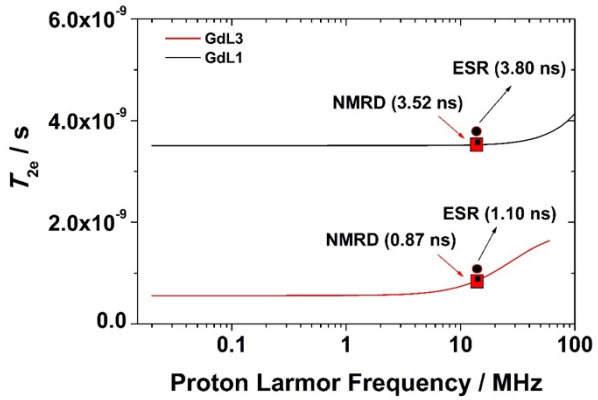

Figure 9 Simulation of the frequency (field) dependence of T_{2e} (line) showing the data points estimated from the independent NMRD and EPR analyses.

Previous research about the factors influencing lanthanide electron spin relaxation in solution remains inconclusive, with suggestions of links to the local metal ion symmetry and overall complex rigidity.[38, 44-46] There must be some mechanism that allows coupling of the electron magnetic moment with the surrounding "lattice", as suggested by Orbach, when considering behaviour in the solid-state.[47] What is becoming clear is that the sensitivity of the ligand donor atoms to perturbation can change the *f* electron-nuclear interaction, and thereby influence the values of T_{1e} and T_{2e}. Moreover, the nature of the solvent plays a key role, even in these coordinatively saturated complexes, as the local solvation shell will determine the relative size of the transient or *dynamic* ligand field. [25,26] Such a contribution is more likely to be manifested in complexes with a small static ligand field parameter B_0^2.

Conclusions

The analysis of the ^{1}H NMR spectra of three series of lanthanide (III) complexes, [Ln.L^1], [Ln.L^2] and [Ln.L^3] (Ln=Tb, Dy, Ho, Er, Tm, Yb) has revealed non-systematic behaviour in the lanthanide-induced shift, both within and between each ligand series. Computational calculations have shown that small deviations from C_3 symmetry, which are present in the X-ray structures and DFT optimised geometries, significantly alter the pseudocontact shift field compared to symmetrised geometries. A useful comparison with experimental data is possible only if the magnetic susceptibility tensor is averaged with respect to rotation about the C_3 axis. However, this approach leads to a reasonable agreement with experiment only for the L^3 series, with a complete failure in the case of the L^1 series. Such a striking disagreement cannot be attributed to the nature of the computational methods themselves, which have proved to be successful in PCS predictions for Ln complexes with much larger ligand fields.[35]

The complex [Gd.L^1] possesses an unusually long electron spin relaxation time. It is an excellent choice as the basis for the development of EPR spectroscopic probes in water, as it gives rise to the narrowest EPR signal of any complex. Indeed, the ease of perturbation of the ligand field in the complexes of L^1 and its derivatives, suggests that these systems are well suited as the basis for responsive probe design, *e.g.* in creating new Gd spin-labels for double electron-electron resonance (DEER)[48], and paramagnetic NMR applications. [25]

Experimental

Materials and Structural data. All complexes have been prepared as described earlier. The crystallographic data for the structures discussed here have been deposited at the Cambridge Crystallographic Data Centre.[13, 14, 18-20, 32] For the lanthanide complexes of L^1, see CCDC 206376-206378 and 1850294; for the Eu, Ho, Tm and Yb structures of L^2 see: CCDC 836097, 836098, 836101 and 836102; for complexes of L^3 see: 965909–965911 and CCDC-1879271, 1879268, 1879264, 1879265, 1879272, 1879266, 1879267, 1879270.

EPR Spectroscopy. EPR spectra were recorded using JEOL FA-200 EPR X-band spectrometer with a JEOL ES-LC11 flat cell for aqueous sample analysis. Spectra were recorded under the following conditions: magnetic field 347 ± 250 mT; field modulation depth 0.6 mT; field modulation frequency 100 kHz; time constant 0.03 s; sweep time 1 min; microwave frequency 9.451 GHz, microwave power 2 mW. Three scans were accumulated for each sample. The temperature of the sample was controlled with a JEOL DVT airflow heater equipped with a calibrated copper-constantan thermocouple. A solid sample of the meglumine (D(-)-*N*-methylglucamine) salt of [Gd.DOTA]$^-$ has been kindly provided by Bracco Imaging S.p.A. (Colleretto Giacosa, Italy). mp 137 °C dec. Anal. Calcd (found) for $C_{31}H_{50}GdN_5O_{14}$: C, 42.56 (42.42); H, 5.76 (5.96); Gd, 17.99 (17.63); N, 8.01 (7.72). An aqueous solution of the complex (0.5 mM) was used after adjusting the pH to 7.3 with 0.2 N aq. NaOH solution.

NMR measurements and fitting. ^{1}H, NMR spectra were recorded in commercially available deuterated solvents using a Varian VNMRS-700 spectrometer (^{1}H at 699.73 MHz). The NMR shift data for the corresponding yttrium complex of each ligand was used to subtract the diamagnetic contributions to the total chemical shift. Paramagnetic shifts were assigned and fitted to extract susceptibility tensors using averaged DFT computed hyperfine tensors following eq. 18 from the work of Kuprov [28] as implemented in Spinach.[49]

Computational details. Geometry optimisation was done with M06-2X functional[50] with cc-pVDZ basis set[51] and Stuttgart ECP[52, 53] for Ln. Solvent effects were accounted for with the SMD continuum model[54] for methanol, and an additional empirical dispersion correction GD3[55] was introduced to account for weak interactions using the Gaussian 09 program.[56]

Complete active space self-consistent field with account for spin-orbit coupling (CASSCF-SO) calculations were performed with MOLCAS 8.0[57] using the CASSCF/RASSI/SINGLE_ANISO approach,[58] employing structures as determined by DFT optimization omitting non-coordinating solvent molecules and counter ions. In all calculations the Ln atoms were treated with the ANO-RCC-VTZP basis, the N and O donor atoms with the

ANO-RCC-VDZP basis, while all other atoms were treated with the ANO-RCC-VDZ basis.[59] In order to save disk space the two electron integrals were decomposed using the Cholesky decomposition with a threshold of 10^{-8}. The electronic configurations of Tb^{III} ($4f^{8}$), Dy^{III} ($4f^{9}$), Ho^{III} ($4f^{10}$), Er^{III} ($4f^{11}$), Tm^{III} ($4f^{12}$), and Yb^{III} ($4f^{13}$) were modelled with a complete active space of 8, 9, 10, 11, 12, and 13 electrons, respectively, in the 7 4*f* orbitals. The spin multiplets that were included in the RASSCF orbital optimization of the spin-only wave functions as well as the number of states mixed by spin-orbit coupling by RASSI are reported in Table S2. The SINGLE_ANISO module was used to compute the magnetic properties of the complexes and to obtain the CFPs by projecting the lowest lying CASSCF-SO wave functions onto a (2*J* + 1)-dimensional pseudo-spin basis.[11]

^{1}H NMRD measurements. The proton $1/T_1$ NMRD profiles were measured on a fast field-cycling Stelar SmartTracer relaxometer (Mede, Pavia, Italy) over a continuum of magnetic field strengths from 0.00024 to 0.25 T (corresponding to 0.01-10 MHz proton Larmor frequencies). The relaxometer operates under computer control with an absolute uncertainty in $1/T_1$ of ± 1%. The temperature control was carried out using a Stelar VTC-91 airflow heater equipped with a calibrated copper–constantan thermocouple (uncertainty of ±0.1 K). Additional data points in the range 20-70 MHz were obtained on a Stelar Relaxometer equipped with a Bruker WP80 NMR electromagnet adapted to variable-field measurements (15-80 MHz proton Larmor frequency). The exact complex concentration was determined by the BMS shift method at 11.7 T.[60]

Conflicts of interest

There are no conflicts to declare.

Acknowledgements

We acknowledge preliminary work of A. Funk and S. Worswick, and thank EPSRC for support (EP/N 006909/1; EP/L01212X; EP/N007 6985/1).

References

1. G. Cucinotta, M. Perfetti, J. Luzon, M. Etienne, P.-E. Car, A. Caneschi, G. Calvez, K. Bernot and R. Sessoli, *Angew. Chem. Int. Ed.*, 2012, **124**, 1638-1642.
2. L. Rigamonti, A. Nava, M.-E. Boulon, J. Luzon, R. Sessoli and A. Cornia, *Chem.. Eur. J.* 2015, **21**, 12171-12180.
3. A. B. Canaj, M. K. Singh, C. Wilson, G. Rajaraman and M. Murrie, *Chem. Commun.*, 2018, **54**, 8273-8276.
4. J. D. Rinehart and J. R. Long, *Chem. Sci.*, 2011, **2**, 2078-2085.
5. D. Esteban-Gómez, L. A. Büldt, P. Pérez-Lourido, L. Valencia, M. Seitz and C. Platas-Iglesias, *Inorg. Chem.*, 2019, **58**, 3732-3743.
6. M. Autillo, L. Guerin, T. Dumas, M. S. Grigoriev, A. M. Fedoseev, S. Cammelli, P. L. Solari, D. Guillaumont, P. Guilbaud, P. Moisy, H. Bolvin and C. Berthon, *Chem. Eur. J.*, 2019, **25**, 4435-4451.
7. J.-Q. He, S.-F. Xie, B.-L. Lai, M. Yang, W.-B. Chen, Y.-Q. Zhang and W. Dong, *Dalton Trans.*, 2018, **47**, 14975-14984.
8. M. Hiller, S. Krieg, N. Ishikawa and M. Enders, *Inorg. Chem.*, 2017, **56**, 15285-15294.
9. M. Perfetti, M. Gysler, Y. Rechkemmer-Patalen, P. Zhang, H. Taştan, F. Fischer, J. Netz, W. Frey, L. W. Zimmermann, T. Schleid, M. Hakl, M. Orlita, L. Ungur, L. Chibotaru, T. Brock-Nannestad, S. Piligkos and J. van Slageren, *Chem. Sci.*, 2019, **10**, 2101-2110.
10. E. Kreidt, C. Bischof, C. Platas-Iglesias and M. Seitz, *Inorg. Chem.*, 2016, **55**, 5549-5557.
11. L. Ungur and L. F. Chibotaru, *Chem. Eur. J.*, 2017, **23**, 3708-3718.
12. M. Böhme and W. Plass, *J. . Comp. Chem.*, 2018, **39**, 2697-2712.
13. S. J. Butler, M. Delbianco, L. Lamarque, B. K. McMahon, E. R. Neil, R. Pal, D. Parker, J. W. Walton and J. M. Zwier, *Dalton Trans.*, 2015, **44**, 4791-4803.
14. E. R. Neil, A. M. Funk, D. S. Yufit and D. Parker, *Dalton Trans.*, 2014, **43**, 5490-5504.
15. M. Starck, R. Pal and D. Parker, *Chem. Eur. J.*, 2016, **22**, 570-580.
16. D. Parker, in *Handbook on the Physics and Chemistry of Rare Earths*, Elsevier, 2016, vol. 50, pp. 269-299.
17. D. Parker, R. S. Dickins, H. Puschmann, C. Crossland and J. A. Howard, *Chem. Rev.*, 2002, **102**, 1977-2010.
18. G. Nocton, A. Nonat, C. Gateau and M. Mazzanti, *Helv. Chim. Acta*, 2009, **92**, 2257-2273.
19. C. Gateau, M. Mazzanti, J. Pécaut, F. A. Dunand and L. Helm, *Dalton Trans.*, 2003, 2428-2433.
20. J. W. Walton, L. Di Bari, D. Parker, G. Pescitelli, H. Puschmann and D. S. Yufit, *Chem. Commun.* 2011, **47**, 12289-12291.
21. B. Bleaney, *J. Mag. Res. (1969)*, 1972, **8**, 91-100.
22. I. Bertini, C. Luchinat and G. Parigi, *Progress in Nuclear Magnetic Resonance Spectroscopy*, 2002, **40**, 249-273.
23. A. M. Funk, K.-L. N. A. Finney, P. Harvey, A. M. Kenwright, E. R. Neil, N. J. Rogers, P. Kanthi Senanayake and D. Parker, *Chem. Sci.*, 2015, **6**, 1655-1662.
24. M. Vonci, K. Mason, E. A. Suturina, A. T. Frawley, S. G. Worswick, I. Kuprov, D. Parker, E. J. L. McInnes and N. F. Chilton, *J. Am. Chem. Soc.*, 2017, **139**, 14166-14172.
25. K. Mason, A. C. Harnden, C. W. Patrick, A. W. J. Poh, A. S. Batsanov, E. A. Suturina, M. Vonci, E. J. L. McInnes, N. F. Chilton and D. Parker, *Chem. Commun.*, 2018, **54**, 8486-8489.
26. M. Vonci, K. Mason, E. R. Neil, D. S. Yufit, E. J. L. McInnes, D. Parker and N. F. Chilton, *Inorg. Chem.*, 2019, DOI: 10.1021/acs.inorgchem.9b00060.
27. E. A. Suturina, K. Mason, C. F. G. C. Geraldes, I. Kuprov and D. Parker, *Angew. Chem. Int. Ed.*, 2017, **56**, 12215-12218.
28. E. A. Suturina and I. Kuprov, *Phys. Chem. Chem.Phys.* 2016, **18**, 26412-26422.
29. A. J. Pell, G. Pintacuda and C. P. Grey, *Progress in Nuclear Magnetic Resonance Spectroscopy*, 2019, **111**, 1-271.
30. A. M. Funk, P. H. Fries, P. Harvey, A. M. Kenwright and D. Parker, *J. Phys. Chem. A*, 2013, **117**, 905-917.

31. J. H. Freed, *J. Chem. Phys.*, 1978, **68**, 4034-4037.
32. J. W. Walton, R. Carr, N. H. Evans, A. M. Funk, A. M. Kenwright, D. Parker, D. S. Yufit, M. Botta, S. De Pinto and K.-L. Wong, *Inorg. Chem.*, 2012, **51**, 8042-8056.
33. D. H. Powell, O. M. N. Dhubhghaill, D. Pubanz, L. Helm, Y. S. Lebedev, W. Schlaepfer and A. E. Merbach, *J. Am. Chem. Soc.*, 1996, **118**, 9333-9346.
34. N. Bloembergen and L. O. Morgan, *J.Chem Phys.* 1961, **34**, 842-850.
35. L. Helm, *Progress in Nuclear Mag. Reson. Spec.*, 2006, **49**, 45-64.
36. S. Aime, A. Barge, M. Botta, M. Fasano, J. Danilo Ayala and G. Bombieri, *Inorg. Chim.Acta*, 1996, **246**, 423-429.
37. S. H. Koenig and R. D. Brown, *Progress in Nuclear Magnetic Resonance Spectroscopy*, 1990, **22**, 487-567.
38. P. Caravan, J. J. Ellison, T. J. McMurry and R. B. Lauffer, *Chem. Rev.*, 1999, **99**, 2293-2352.
39. J. Reuben, *J.Phys. Chem.*, 1971, **75**, 3164-3167.
40. D. H. Powell, A. E. Merbach, G. González, E. Brücher, K. Micskei, M. F. Ottaviani, K. Köhler, A. Von Zelewsky, O. Y. Grinberg and Y. S. Lebedev, *Helv. Chim. Acta*, 1993, **76**, 2129-2146.
41. R. B. Clarkson, A. I. Smirnov, T. I. Smirnova, H. Kang, R. L. Belford, K. Earle and J. H. Freed, *Mol. Phys.*, 1998, **95**, 1325-1332.
42. A. Borel, É. Tóth, L. Helm, A. Jánossy and A. E. Merbach, *Phys. Chem. Chem. Phys.*, 2000, **2**, 1311-1317.
43. A. Borel, H. Kang, C. Gateau, M. Mazzanti, R. B. Clarkson and R. L. Belford, *J. Phys. Chem. A*, 2006, **110**, 12434-12438.
44. I. Bertini, F. Capozzi, C. Luchinat, G. Nicastro and Z. Xia, *J. Phys. Chem.*, 1993, **97**, 6351-6354.
45. C. B. P. Finn, R. Orbach and W. P. Wolf, *Proc. Phys. Soc.*, 1961, **77**, 261-268.
46. M. R. Jensen and J. J. Led, *J. Mag. Reson.*, 2004, **167**, 169-177.
47. R. Orbach, *Proc.s Phys. Soc.*, 1961, **77**, 821-826.
48. A. Shah, A. Roux, M. Starck, J. A. Mosely, M. Stevens, D. G. Norman, R. I. Hunter, H. El Mkami, G. M. Smith, D. Parker and J. E. Lovett, *Inorg. Chem.*, 2019, **58**, 3015-3025.
49. H. J. Hogben, M. Krzystyniak, G. T. P. Charnock, P. J. Hore and I. Kuprov, *Journal of Magnetic Resonance*, 2011, **208**, 179-194.
50. Y. Zhao and D. G. Truhlar, *Theoretical Chemistry Accounts: Theory, Computation, and Modeling (Theoretica Chimica Acta)*, 2008, **120**, 215-241.
51. T. H. Dunning Jr, *J. Chem. Phys.*, 1989, **90**, 1007-1023.
52. K. L. Schuchardt, B. T. Didier, T. Elsethagen, L. Sun, V. Gurumoorthi, J. Chase, J. Li and T. L. Windus, *J. Chem.l Inf. Mod.*, 2007, **47**, 1045-1052.
53. M. Dolg, H. Stoll, H. Preuss and R. M. Pitzer, *J. Phys. Chem.*, 1993, **97**, 5852-5859.
54. A. V. Marenich, C. J. Cramer and D. G. Truhlar, *J. Phys. Chem. B*, 2009, **113**, 6378-6396.
55. S. Grimme, J. Antony, S. Ehrlich and H. Krieg, *J. Chem. Phys.*, 2010, **132**, 154104.
56. Gaussian 09, Revision D.01, M. J. Frisch, G. W. Trucks, H. B. Schlegel, G. E. Scuseria, M. A. Robb, J. R. Cheeseman, G. Scalmani, V. Barone, B. Mennucci, G. A. Petersson, H. Nakatsuji, M. Caricato, X. Li, H. P. Hratchian, A. F. Izmaylov, J. Bloino, G. Zheng, J. L. Sonnenberg, M. Hada, M. Ehara, K. Toyota, R. Fukuda, J. Hasegawa, M. Ishida, T. Nakajima, Y. Honda, O. Kitao, H. Nakai, T. Vreven, J. A. Montgomery, Jr., J. E. Peralta, F. Ogliaro, M. Bearpark, J. J. Heyd, E. Brothers, K. N. Kudin, V. N. Staroverov, T. Keith, R. Kobayashi, J. Normand, K. Raghavachari, A. Rendell, J. C. Burant, S. S. Iyengar, J. Tomasi, M. Cossi, N. Rega, J. M. Millam, M. Klene, J. E. Knox, J. B. Cross, V. Bakken, C. Adamo, J. Jaramillo, R. Gomperts, R. E. Stratmann, O. Yazyev, A. J. Austin, R. Cammi, C. Pomelli, J. W. Ochterski, R. L. Martin, K. Morokuma, V. G. Zakrzewski, G. A. Voth, P. Salvador, J. J. Dannenberg, S. Dapprich, A. D. Daniels, O. Farkas, J. B. Foresman, J. V. Ortiz, J. Cioslowski, and D. J. Fox, Gaussian, Inc., Wallingford CT, 2013.
57. F. Aquilante, J. Autschbach, R. K. Carlson, L. F. Chibotaru, M. G. Delcey, L. De Vico, I. Fdez. Galván, N. Ferré, L. M. Frutos, L. Gagliardi, M. Garavelli, A. Giussani, C. E. Hoyer, G. Li Manni, H. Lischka, D. Ma, P. Å. Malmqvist, T. Müller, A. Nenov, M. Olivucci, T. B. Pedersen, D. Peng, F. Plasser, B. Pritchard, M. Reiher, I. Rivalta, I. Schapiro, J. Segarra-Martí, M. Stenrup, D. G. Truhlar, L. Ungur, A. Valentini, S. Vancoillie, V. Veryazov, V. P. Vysotskiy, O. Weingart, F. Zapata and R. Lindh, *J. Comp. Chem.*, 2016, **37**, 506-541.
58. L. F. Chibotaru and L. Ungur, *J. Chem. Phys.*, 2012, **137**, 064112.
59. B. O. Roos, R. Lindh, P.-Å. Malmqvist, V. Veryazov and P.-O. Widmark, *J. Phys. Chem. A*, 2005, **109**, 6575-6579.
60. B. A. Corbin, A. C. Pollard, M. J. Allen and M. D. Pagel, *Molecular Imaging and Biology*, 2019, DOI: 10.1007/s11307-019-01315-8.